Pulse Shaping for Backscatter Radio

John Kimionis
School of Electrical and
Computer Engineering
Georgia Institute of Technology
Atlanta, GA 30308
Email: ikimionis@gatech.edu

Manos M. Tentzeris
School of Electrical and
Computer Engineering
Georgia Institute of Technology
Atlanta, GA 30308
Email: etentze@ece.gatech.edu

Abstract—**Backscatter radio is being increasingly used for identification, sensing, and localization. The increased number of pervasive IoT systems that utilize backscatter radio as a low-power and low-cost communication scheme has led to dense deployments of tags that need to operate under bandwidth constraints. However, typical backscatter radio modulators perform switching "on-off" operation and modulate data with rectangular pulses, which are known to occupy an extensively wide bandwidth. This work derives new techniques and demonstrates front-ends that control the tag reflection coefficient over time in a continuous manner, thus enabling the generation of arbitrary backscattered waveforms and reduced bandwidth occupancy. The principles presented hereby will enable sophisticated tags to perform more complex modulation schemes, while maintaining the RF front-end complexity at low levels, using a single PIN diode or FET.**

Index Terms—**Backscatter radio, pulse shaping, spectral efficiency, RF front-end, RFID, IoT**

I. INTRODUCTION

In dense backscatter tag deployments, e.g. for sensor networks, minimizing the utilized bandwidth per tag is crucial for the scalability of the system. Specifically, being able to fit large number of sensors in adjacent frequency channels requires that each tag's backscattered signal spectrum decays fast in frequency. Ideally, the signal's harmonics have to be suppressed so that they do not interfere with nearby channel sensors' responses. Active radio systems utilize pulse shaping techniques to modify the waveform characteristics of the transmitted signals and adapt them according to the requirements of bandwidth, datarate, etc. Although conventional radio utilizes complex electronic components to achieve shaping, backscatter radio typically utilizes minimal RF front-ends consisting of only one or a few nonlinear devices (switches, transistors, diodes) that switch between discrete states. However, this is not a strongly-limiting factor for getting away from conventional on-off keying (OOK) modulation on sophisticated sensing RFID tags that employ computational units, such as microcontrollers, at the core of their system. Prior art has exploited multiple load values with RF switches to achieve higher-order modulation constellations [1], albeit still utilizing rectangular pulses and thus extended bandwidth. This work demonstrates how backscatter tags can benefit from low-complexity front-end designs that allow generating arbitrary waveforms. That is achieved by exploiting continuous
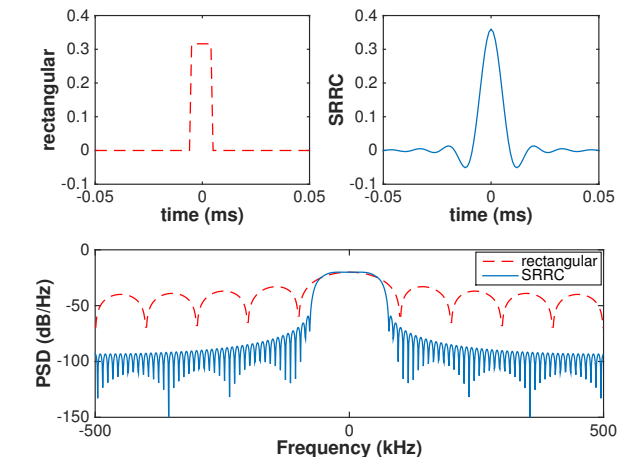
Fig. 1. Spectrum comparison of 100 kbps rectangular pulses (typically used in backscatter radio) and square root raised cosine pulses of the same energy.

variation of the antenna load instead of switching between two discrete values, effectively breaking the limit of rectangular waveforms and high bandwidth occupation.

For a backscatter modulator, the antenna-load system reflection coefficient is

$$\Gamma = \frac{Z_L - Z_a^*}{Z_L + Z_a},\qquad(1)$$

where Z_L and Z_a are the load and antenna impedance, respectively. From [2], the received complex baseband signal at the reader is

$$\tilde{y}(t) = a_{\mathrm{dc}}e^{j\phi_{\mathrm{dc}}} + a_{\mathrm{mod}}e^{j\phi_{\mathrm{mod}}}\Gamma(t-\tau),\qquad(2)$$

where $a_{\mathrm{dc}}e^{j\phi_{\mathrm{dc}}}$ contains all the unmodulated contributions of the received signal (reader's carrier and tag's unmodulated structural scattering) and $a_{\mathrm{mod}}e^{j\phi_{\mathrm{mod}}}$ scales the modulated received tag signal, which is a direct function of Γ over time, delayed by a time constant τ depending on the wireless channel.

Modulation is achieved when $\Gamma(t)$ changes over time, due to changes in the modulator's load impedance. Typically, backscatter load modulators utilize two load values for $\Gamma(t)$ to achieve binary communication. In those cases, at the receiver,
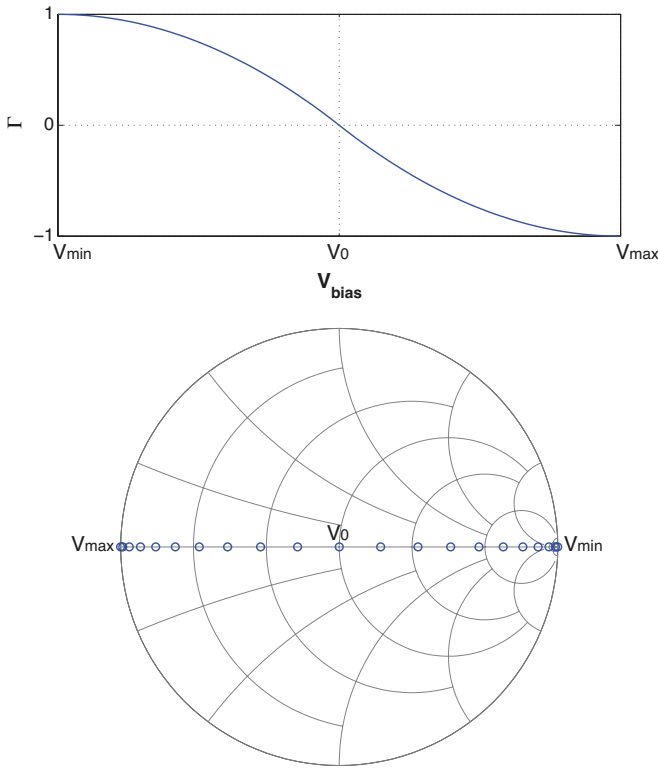
Fig. 2. Reflection coefficient as a function of bias voltage in linear form and impedance representation.

Fig. 3. Reflection coefficient decomposed to magnitude and phase components, defining a positive and a negative reflected signal region.
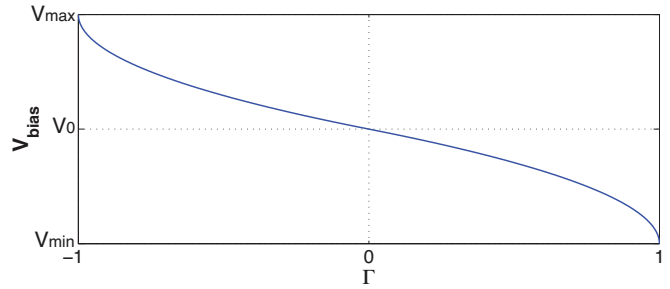
Fig. 4. Inverted function providing the required bias voltage to achieve a certain reflection coefficient value.

the baseband signal $\tilde{y}(t)$ features sharp changes between two (complex, in general) values, i.e. the received signal consists of rectangular pulses. To transmit data at a datarate R, a very large bandwidth W (infinite in theory) is required in the frequency domain with rectangular pulses (Fig. 1), although this bandwidth could be minimized to $W = R$ while maintaining reliable communication without inter-symbol interference, according to the Nyquist criterion [3]. A Nyquist pulse typically used in active radio is the square root raised cosine (SRRC), which, at the expense of longer pulse duration (e.g. 10 times the bit duration $T = 1/R$ in Fig. 1), features a main-lobe bandwidth of $W = (1 + a)/T$, where $0 \leq a \leq 1$ is the roll-off factor that defines how fast the pulse spectrum will decay in frequency. The difference in spectrum occupancy for rectangular and SRRC pulses of the same energy is apparent in Fig. 1-bottom, where the power spectral density (PSD) of the two pulses is shown. Therefore, it is appealing to be able to generate SRRC pulses or other arbitrary waveforms with a simple backscatter front-end, without the need of high-complexity electronics. This can be achieved with a single active element front-end that continuously variates the antenna load to achieve backscatter modulation.

II. CONTINUOUS LOAD VARIATION

Assume a purely resistive load $Z_L = R(V_{\text{bias}})$ controlled by a bias voltage V_{bias} and an antenna impedance $Z_a = 50\ \Omega$.

Then,

$$\Gamma(V_{\text{bias}}) = \frac{R(V_{\text{bias}}) - 50}{R(V_{\text{bias}}) + 50} \tag{3}$$

is a real quantity with $1 \geq \Gamma(V_{\text{bias}}) \geq -1$. Let V_{min} be a low voltage level for which $\Gamma(V_{\text{min}}) = 1$, i.e. the antenna load acts as an open circuit ($R \to \infty$). Similarly, let V_{max} be the voltage level that turns the load to a short circuit ($R = 0\ \Omega$), i.e. $\Gamma(V_{\text{max}}) = -1$. Moreover, let V_0 be the voltage that minimizes the reflection coefficient magnitude $|\Gamma(V_0)| = 0$, which occurs at $R = 50\ \Omega$. The reflection coefficient as a function of the bias voltage is shown in Fig. 2 in linear form and on a Smith Chart, where it can be seen that $\Delta\Gamma$ variations close to the edges of the smith chart (high return loss) are more "dense" in contrast with the ones close to the chart's center, for equidistant variations of the bias voltage ΔV_{bias}. The reflection coefficient can be decomposed to its magnitude and phase components as shown in Fig. 3. It can be seen that the reflection coefficient values can be split to one "positive" region for $V_{\text{bias}} < V_0$ and one "negative"
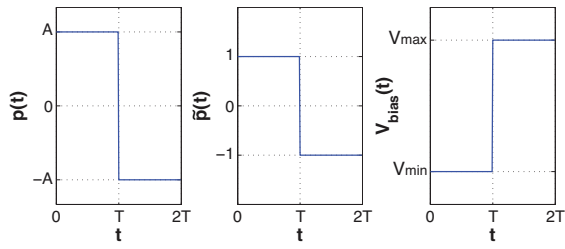
Fig. 5. Transformation of pulse to be transmitted (left) to reflection coefficient values (center) and required bias voltage (right).
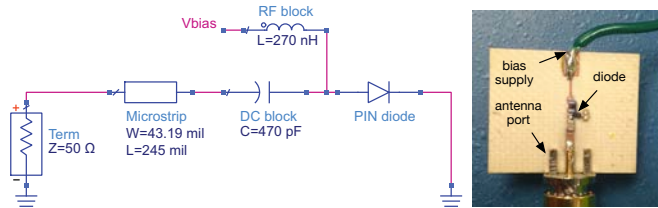
Fig. 6. Pulse shaping front-end schematic (left) and prototype (right).

region for $V_{bias} > V_0$. Assuming an incident RF voltage to the load, a positive or negative voltage of any level can be reflected back by applying the appropriate bias value. Finding the required bias voltage for a certain reflection coefficient requires inverting the function $\Gamma(V_{bias})$, i.e. finding the function $V_{bias}(\Gamma)$. From Fig. 2-top, it can be seen that $\Gamma(V_{bias})$ is a 1-1 function, and thus invertible; the inverse $V_{bias}(\Gamma)$ function is shown in Fig. 4.

Assume we need to transmit an arbitrary pulse $p(t)$, e.g. the one shown in Fig. 5-left. The amplitude level of the pulse is first confined in the interval $[-1, 1]$ with the normalization

$$\tilde{p}(t) = p(t)/\max|p(t)|, \qquad (4)$$

to yield the pulse shown in Fig. 5-center, which is expressed in reflection coefficient values. By using the $V_{bias}(\Gamma)$ function in Fig. 4, $\tilde{p}(t)$ can be translated to the bias voltage required to yield this reflection coefficient variation over time. The result is the voltage function over time shown in Fig. 5-right.

III. Pulse Shaping Front-end Implementation

The front-end consists of a single active element that features a voltage-controlled resistance behavior. As a proof of concept, a PIN diode that is targeted to variable attenuator applications is used. A similar mechanism can be also implemented with a field-effect transistor (FET), since it shows a drain–source resistance variation that is dependent of the gate voltage.

The pulse shaping front-end consists of a single attenuator PIN diode terminated to a short circuit (to achieve maximum reflection with a negative sign $\Gamma_{short} = -1$ when the PIN diode is fully biased and maximum reflection with a positive sign when the diode is not biased and behaves as an RF open $\Gamma_{open} = 1$) and a DC bias/DC block network (Fig. 6-left). The front-end is analyzed with Keysight ADS utilizing a non-linear SPICE model for the diode, manufacturer models for
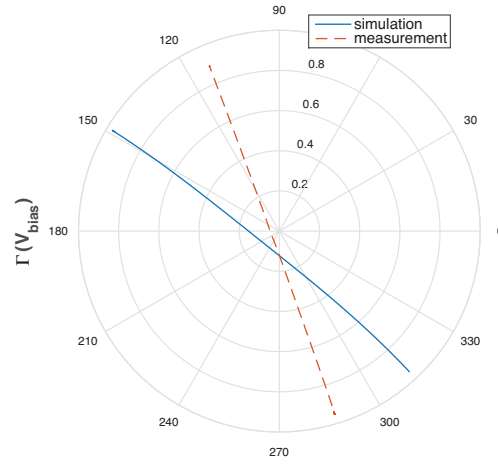
Fig. 7. Reflection coefficient versus bias voltage level (0–1 Volts).

the lumped components, and full-wave simulation of the PCB layout and the feeding microstrip line. The simulated $\Gamma(V_{bias})$ is shown in Fig. 7. Compared to the analytical plot of Fig. 2, the curve shows a phase shift and a small offset from the center of the polar plot. These practically do not affect the received signal at the reader, since the offset will contribute to the DC term of Eq. (2), and the phase shift will be absorbed by the already-present phase term $e^{j\phi_{mod}}$ that rotates $\Gamma(t - \tau)$ in the complex plane.

The front-end is implemented on a thin laminate substrate (Fig. 6-right) and is characterized using an automated setup of continuous bias voltage sweeping with a data acquisition (DAQ) unit and S-parameter measurements with a vector network analyzer (VNA). The measured reflection coefficient for a bias voltage range of 0 to 1 Volts features a similar behavior with the simulated data (Fig. 7), with an introduced phase shift which, as mentioned previously, does not affect signal detection at the reader.

IV. Measurements

To test the pulse shaping front-end, an experimental setup has been utilized, consisting of a full-duplex software-defined radio (SDR) whose Tx and Rx ports are connected to a UHF circulator; the front-end is wired to the third circulator port. The SDR generates a continuous wave (CW) at 913 MHz which excites the front-end and the response is received by the SDR. An SRRC pulse with rolloff factor $\alpha = 0.5$ is generated to pulse shape pseudorandom generated data (Fig. 8-top). The pulse is scaled to $\Gamma \in [-1, 1]$ interval and is translated to the required V_{bias} using the measured $V_{bias}(\Gamma)$ data (Fig. 8-bottom). A DAQ is driving the front-end with the waveform of 50 pulse-shaped data bits, and the SDR implements a receiver with SRRC matched filtering, bit-level synchronization, and detection to verify the accurate generation of backscatter SRRC pulses. For wireless measurements, the front-end is detached from the circulator and is connected to a UHF antenna. The third port of the circulator also hosts an antenna
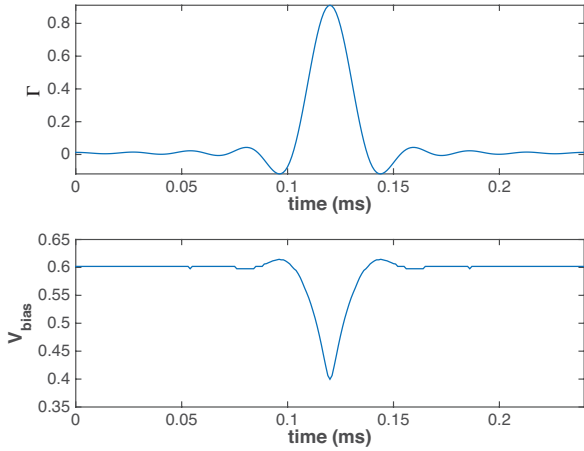
Fig. 8. SRRC pulse in reflection coefficient and bias voltage representation.

Fig. 9. Backscatter signals in time domain. Top: conventional rectangular pulses. Center: SRRC pulses with proposed front-end. Bottom: wireless reception.

for wireless transmission and reception from the SDR at the 900-MHz band.

For bandwidth comparison, a front-end consisting of a simple on-off RF switch is tested with the same bitstream. In Fig. 9-top, the bitstream is shown, modulated with conventional rectangular pulses. In Fig. 9-center and Fig. 9-bottom, the SDR-received backscattered SRRC pulses are shown for wired and wireless cases, respectively. The backscattered SRRC pulses are smooth, showcasing the continuity of $\Gamma(t)$ achieved with the designed front-end, and are successfully decoded by the SDR receiver after matched filtering. The spectrum of the received rectangular pulse-modulated data is shown in Fig. 10 across with the spectrum of the SRRC-shaped data for a datarate of $R = 100$ kbps. It is apparent that the power decay is sharper for backscatter SRRC-shaping, reaching a power suppression of up to 35 dB out-of-band (for the same received pulse energy), leaving more free bandwidth for adjacent tags/sensors. Moreover, the SDR-captured spectrum of the backscattered SRRC-shaped data occupies a two-sided frequency window that matches with the theoretical bandwidth of SRRC: $W = (1 + \alpha)R = 150$ kHz.

V. CONCLUSION

The feasibility of generating arbitrary waveforms to enable pulse shaping with backscatter radio for "dense" RFID, sensing, and IoT applications was discussed. The principle of continuously varying the tag reflection coefficient and how this translates to pulse-shaped backscatter signals was analyzed and demonstrated with a front-end that maintains a very low complexity, utilizing a single non-linear component. The operation of the front-end was verified by successful reception and demodulation of pulse-shaped backscatter signals with a SDR reader, as well as by examining the bandwidth occupancy of pulse-shaped signals and contrasting with the respective spectrum occupancy of typically-used rectangular pulse-modulated backscatter. The principles of this work will enable smart backscatter sensors and computational RFID to
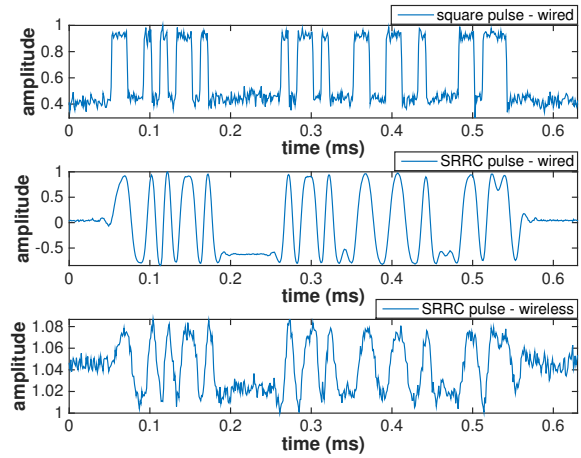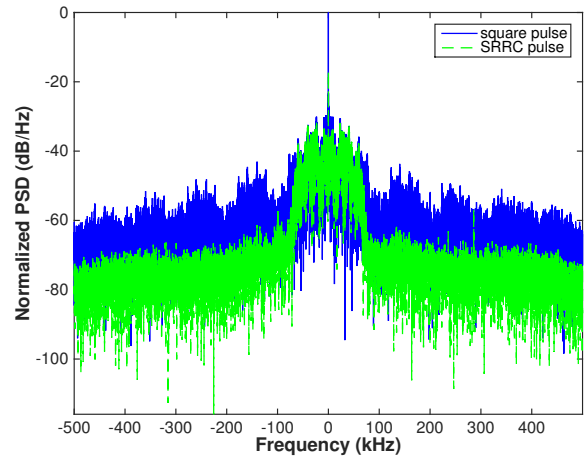
Fig. 10. Spectrum comparison of wireless SDR-received backscatter rectangular pulse and SRRC pulse-shaped backscatter. The strong DC peak corresponds to the reader's CW that illuminates the backscatter modulator.

perform complex modulation schemes with reduced bandwidth occupancy, and thus higher spectral efficiency.

REFERENCES

[1] S. Thomas, E. Wheeler, J. Teizer, and M. Reynolds, "Quadrature amplitude modulated backscatter in passive and semipassive UHF RFID systems," *IEEE Trans. Microw. Theory Techn.*, vol. 60, no. 4, pp. 1175–1182, Apr. 2012.

[2] J. Kimionis, A. Bletsas, and J. N. Sahalos, "Increased range bistatic scatter radio," *IEEE Trans. Commun.*, vol. 62, no. 3, pp. 1091–1104, Mar. 2014.

[3] J. G. Proakis, *Digital Communications*, 4th ed. New York, NY, 10020: McGraw-Hill, Inc., 2001.